

## 11 $\beta$ -Hydroxysteroid dehydrogenase blockade prevents age-induced skin structure and function defects

Ana Tiganescu, ... , Gareth G. Lavery, Paul M. Stewart

*J Clin Invest.* 2013;123(7):3051-3060. <https://doi.org/10.1172/JCI64162>.

Research Article

Aging

Glucocorticoid (GC) excess adversely affects skin integrity, inducing thinning and impaired wound healing. Aged skin, particularly that which has been photo-exposed, shares a similar phenotype. Previously, we demonstrated age-induced expression of the GC-activating enzyme 11 $\beta$ -hydroxysteroid dehydrogenase type 1 (11 $\beta$ -HSD1) in cultured human dermal fibroblasts (HDFs). Here, we determined 11 $\beta$ -HSD1 levels in human skin biopsies from young and older volunteers and examined the aged 11 $\beta$ -HSD1 KO mouse skin phenotype. 11 $\beta$ -HSD1 activity was elevated in aged human and mouse skin and in PE compared with donor-matched photo-protected human biopsies. Age-induced dermal atrophy with deranged collagen structural organization was prevented in 11 $\beta$ -HSD1 KO mice, which also exhibited increased collagen density. We found that treatment of HDFs with physiological concentrations of cortisol inhibited rate-limiting steps in collagen biosynthesis and processing. Furthermore, topical 11 $\beta$ -HSD1 inhibitor treatment accelerated healing of full-thickness mouse dorsal wounds, with improved healing also observed in aged 11 $\beta$ -HSD1 KO mice. These findings suggest that elevated 11 $\beta$ -HSD1 activity in aging skin leads to increased local GC generation, which may account for adverse changes occurring in the elderly, and 11 $\beta$ -HSD1 inhibitors may be useful in the treatment of age-associated impairments in dermal integrity and wound healing.

Find the latest version:

<https://jci.me/64162/pdf>





# 11 $\beta$ -Hydroxysteroid dehydrogenase blockade prevents age-induced skin structure and function defects

Ana Tiganeşcu,<sup>1</sup> Abd A. Tahrani,<sup>1</sup> Stuart A. Morgan,<sup>1</sup> Marcela Otranto,<sup>2,3</sup>  
Alexis Desmoulière,<sup>2</sup> Lianne Abrahams,<sup>1</sup> Zaki Hassan-Smith,<sup>1</sup> Elizabeth A. Walker,<sup>1</sup>  
Elizabeth H. Rabbitt,<sup>1</sup> Mark S. Cooper,<sup>1</sup> Kurt Amrein,<sup>4</sup> Gareth G. Lavery,<sup>1</sup> and Paul M. Stewart<sup>1</sup>

<sup>1</sup>Centre for Endocrinology, Diabetes and Metabolism, School of Clinical and Experimental Medicine, College of Medical and Dental Sciences, University of Birmingham, Edgbaston, Birmingham, United Kingdom.

<sup>2</sup>Department of Physiology and EA 6309, Faculty of Pharmacy, University of Limoges, Limoges, France.

<sup>3</sup>Histology and Embryology Department, State University of Rio de Janeiro (UERJ), Rio de Janeiro, Brazil. <sup>4</sup>F. Hoffmann-La Roche, Basel, Switzerland.

**Glucocorticoid (GC) excess adversely affects skin integrity, inducing thinning and impaired wound healing. Aged skin, particularly that which has been photo-exposed, shares a similar phenotype. Previously, we demonstrated age-induced expression of the GC-activating enzyme 11 $\beta$ -hydroxysteroid dehydrogenase type 1 (11 $\beta$ -HSD1) in cultured human dermal fibroblasts (HDFs). Here, we determined 11 $\beta$ -HSD1 levels in human skin biopsies from young and older volunteers and examined the aged 11 $\beta$ -HSD1 KO mouse skin phenotype. 11 $\beta$ -HSD1 activity was elevated in aged human and mouse skin and in PE compared with donor-matched photo-protected human biopsies. Age-induced dermal atrophy with deranged collagen structural organization was prevented in 11 $\beta$ -HSD1 KO mice, which also exhibited increased collagen density. We found that treatment of HDFs with physiological concentrations of cortisol inhibited rate-limiting steps in collagen biosynthesis and processing. Furthermore, topical 11 $\beta$ -HSD1 inhibitor treatment accelerated healing of full-thickness mouse dorsal wounds, with improved healing also observed in aged 11 $\beta$ -HSD1 KO mice. These findings suggest that elevated 11 $\beta$ -HSD1 activity in aging skin leads to increased local GC generation, which may account for adverse changes occurring in the elderly, and 11 $\beta$ -HSD1 inhibitors may be useful in the treatment of age-associated impairments in dermal integrity and wound healing.**

## Introduction

Glucocorticoid (GC) excess, whether of endogenous (e.g., Cushing's syndrome) or exogenous (topical or systemic therapy) origin, is associated with a diverse range of adverse side effects including adipose tissue redistribution, proteolysis, bone resorption, and hyperglycemia manifesting respectively as omental adiposity, muscle weakness, osteoporosis, and insulin resistance (1).

In skin, GC excess leads to marked atrophy with dermal and epidermal thinning according to both human (2–4) and rodent (5, 6) studies. GCs also induce a flattening of the normally undulating “rete ridges” at the dermal-epidermal junction (DEJ) (7). At a cellular level, dermal collagen content in human skin is decreased following topical and systemic GC treatment (3, 8, 9) and is similarly decreased in rats following subcutaneous dexamethasone injection (10). Subsequently, there is a profound increase in the transparency of skin with a tissue paper-like consistency, increased fragility, tearing and bruising (7), increased transepidermal water loss (TEWL) (11), poor wound healing (12, 13), and increased infection risk (14).

Many of these features are also shared with the phenotype of aging skin, including thinning and DEJ flattening (15), decreased dermal cellularity (16), reduced collagen content (17–20), and reduced dermal fibroblast proliferation and collagen secretion in

cells from older donors (18). Consequently, aged skin also suffers from an impaired permeability barrier, with increased TEWL (21), altered mechanical properties (22), delayed wound healing (23, 24), and increased disease prevalence (25).

We hypothesize that with no appreciable changes in circulating cortisol concentrations with age, changes in tissue-specific pre-receptor regulation of local GC availability by 11 $\beta$ -hydroxysteroid dehydrogenase type 1 (11 $\beta$ -HSD1) may explain the phenotypic link between GC excess and aging skin. In intact cells, 11 $\beta$ -HSD1 functions exclusively as an NADPH-dependent oxoreductase, activating cortisol from cortisone. We recently characterized the expression of 11 $\beta$ -HSD1 in human and rodent skin, reporting increased 11 $\beta$ -HSD1 expression in primary human dermal fibroblasts (HDFs) from older donors (26). Increased expression was also detected in donor-matched photo-exposed (PE) versus photo-protected (PP) HDFs (26), suggesting that an increased capacity for local GC activation may represent a novel mediator of age-related changes in skin physiology and function common to both intrinsic and extrinsic aging.

Here, we investigated age-dependent changes in 11 $\beta$ -HSD1 human and murine skin tissue explants. Additionally, we examined alterations in dermal integrity, cellularity, and collagen content in murine skin from age-matched 11 $\beta$ -HSD1-null and WT littermates and report a striking reversal of age-induced dermal morphology in KO mice. We describe the GC-driven changes in collagen biosynthesis, modification, and processing gene expression that may underpin these in vivo observations. Finally, we

**Authorship note:** Gareth G. Lavery and Paul M. Stewart are co-senior authors.

**Conflict of interest:** The authors have declared that no conflict of interest exists.

**Citation for this article:** *J Clin Invest.* 2013;123(7):3051–3060. doi:10.1172/JCI64162.

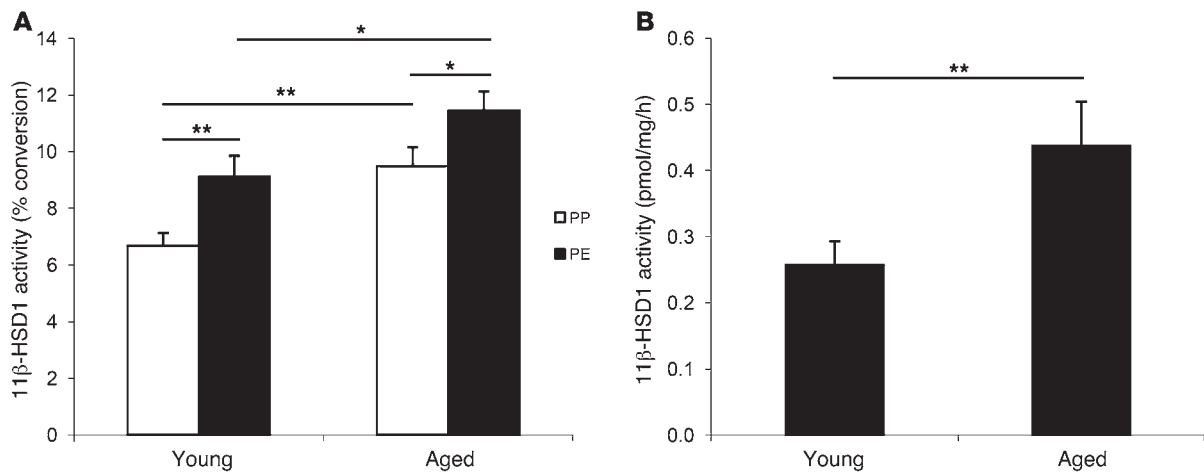


**Figure 1** 11β-HSD1 activity increases in aging skin ex vivo. (A) 11β-HSD1 activity (percentage of conversion of 100 nM cortisone to cortisol) was greater in aged (>60 years) versus young (20–30 years) human skin in both PP (n = 20) and PE (n = 20) biopsies. Activity was also greater in donor-matched PE versus PP samples from young (n = 20) and aged (n = 20) donors. (B) 11β-HSD1 activity (pmol/mg/h) was also greater in older (91–99 weeks; n = 5) versus younger (11–20 weeks; n = 10) mouse skin. \*P < 0.05; \*\*P < 0.01.

demonstrate the translational therapeutic potential of 11β-HSD1 blockade by reporting accelerated wound healing in young mice treated with a selective 11β-HSD1 inhibitor and in aged 11β-HSD1 KO mice relative to their WT littermates.

**Results**

*11β-HSD1 expression increases in aging skin.* 11β-HSD1 activity in human skin obtained from older versus younger donors increased by 42% and 26% in PP and PE biopsies, respectively (Figure 1A). Interestingly, activity in donor-matched PE versus PP samples was also elevated by 36% and 21% in young and aged donors, respec-

tively (Figure 1A). These results using intact tissue are in agreement with our previous observations in cultured HDFs (26). Moreover, 11β-HSD1 activity was 69% higher in aged mouse skin tissue explants (Figure 1B), supporting our human tissue findings and suggesting that increased 11β-HSD1 levels in aged skin are a common feature of mammalian aging.

Furthermore, immunohistochemical studies identified increased 11β-HSD1 protein expression in dermal fibroblasts from PE relative to donor-matched PP skin sections, with increased expression also observed in the epidermal compartment (Figure 2, A and B). Analysis of 11β-HSD1 staining in PE sections

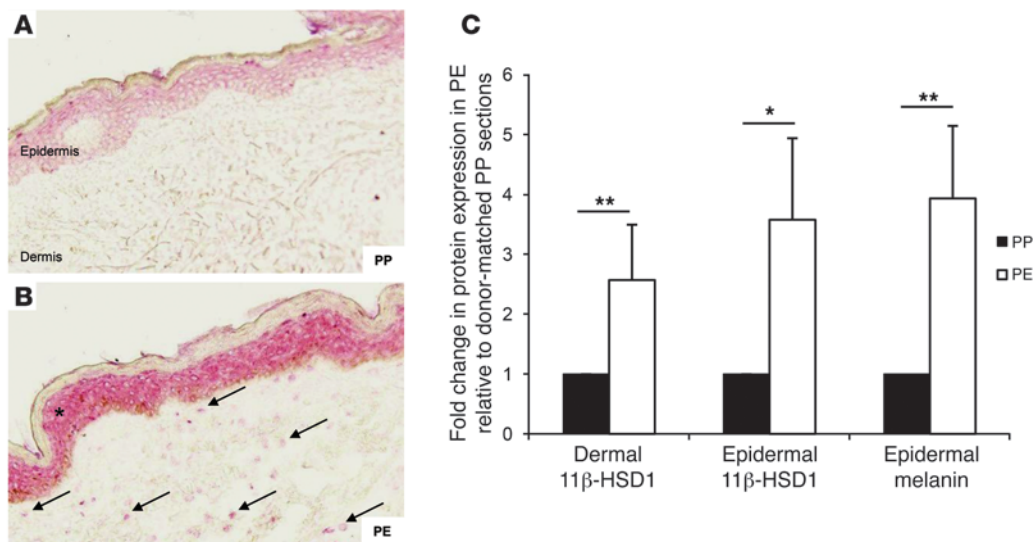


**Figure 2** 11β-HSD1 expression increases in PE skin. 11β-HSD1 staining was increased in epidermal keratinocytes (asterisk) and dermal fibroblasts (arrows) in PE sections (B) relative to donor-matched PP (A) sections (n = 14). Original magnification, ×20. (C) Quantification of tissue staining confirmed elevated dermal and epidermal 11β-HSD1 protein expression (fold change in PE relative to PP sections; n = 14). Endogenous epidermal melanin was used as a positive control and showed the expected increased staining in PE versus PP samples (n = 18). \*P < 0.05; \*\*P < 0.01.

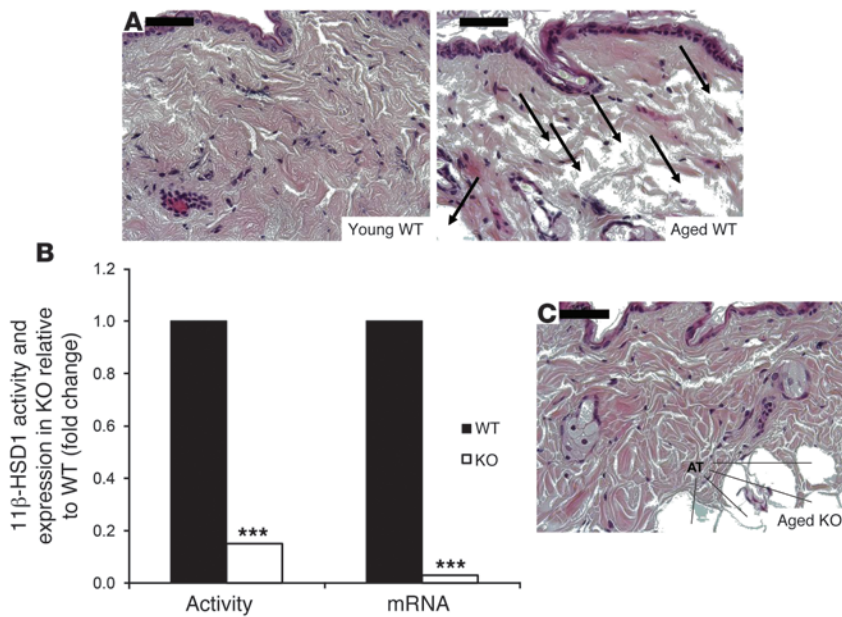


**Figure 3** Reversal of dermal atrophy in aged 11 $\beta$ -HSD1-null mice. (A) Comparison of young and aged WT skin sections ( $n = 4$ ) revealed a grossly altered dermal organization of collagen in the latter, with a loss of structure and tissue integrity (arrows). (B) 11 $\beta$ -HSD1 activity ( $n = 15$ ) and mRNA ( $n = 6$ ) were negligible in 11 $\beta$ -HSD1-null mouse skin compared with WT littermates ( $n = 3$ ). (C) Aged KO mice displayed a striking improvement in dermal structural organization compared with their WT littermates, reverting to a phenotype more comparable to young mice. AT = adipose tissue. Scale bars: 50  $\mu$ M. \*\*\* $P < 0.001$ .

confirmed a 2.5-fold and 3.5-fold increase in dermal and epidermal expression, respectively (Figure 2C), and a 4-fold increase in endogenous epidermal melanin staining (internal control). We also examined the expression of hexose-6-phosphate dehydrogenase, the enzyme supplying NADPH cofactor for 11 $\beta$ -HSD1, and the GC receptor, but found them to be unaffected by donor age and site in human skin or by age and 11 $\beta$ -HSD1 KO in mice (data not shown).

**Reversal of dermal atrophy in aged 11 $\beta$ -HSD1 KO mice.** Aged WT mouse skin displayed a loose collagen network with noticeable atrophy and a sponge-like appearance characterized by large, vacant interfibril spaces (Figure 3A). In some areas of tissue sections from aged mice, the collagen meshwork appeared shredded, with little or no structural integrity or organization. 11 $\beta$ -HSD1 activity in KO mouse skin was reduced to background levels, with negligible mRNA expression (Figure 3B). Strikingly, aged KO mice displayed a histological skin profile more comparable to that of the young WT littermates compared with the aged WT littermates, with improved dermal integrity and more orderly collagen organization (Figure 3C).

Collagen density as assessed with Masson trichrome staining was also improved in 11 $\beta$ -HSD1 KO (Figure 4B) compared with WT mice (Figure 4A). Quantification of collagen staining intensity revealed a 2-fold increase in the aged KO mice (Figure 4C).

**GC regulation of collagen biosynthesis and processing gene expression.** Our *in vivo* studies identified dermal collagen integrity and structural organization as important GC targets in aging skin. The regulation of collagen homeostasis (e.g., posttranslational modification,

transport, and extracellular maturation) by physiological concentrations of endogenous GC had not been previously investigated. Cortisol treatment (100 nM) in HDFs ( $n = 5$ ) downregulated mRNA expression of genes at various stages in the synthesis and processing of mature collagen (Table 1). These included prolyl (*LEPREL1*, *LEPREL2*, and *P4HA2*, with an 80%, 33%, and 36% decrease, respectively) and lysyl (*PLOD2*; 53% decrease) hydroxylases, which hydroxylate the proline and lysine residues on nascent collagen propeptides that facilitate helical trimeric procollagen assembly. We also noted a trend toward reduced expression of *LEPRE1*, *P4HB*, and *PLOD1* hydroxylase mRNA.

The transport and secretion of newly formed procollagen helices are assisted by the collagen-specific chaperone HSP47 (*SERPINH1*), which also exhibited reduced expression follow-

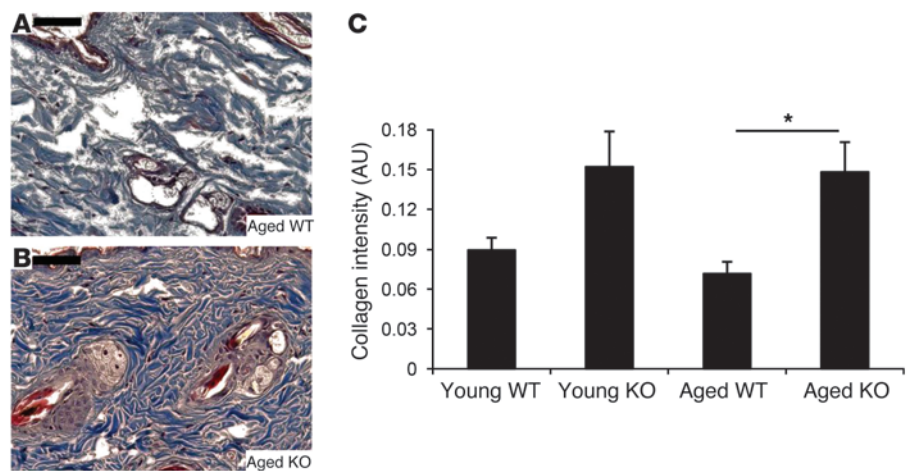


**Figure 4** Improved collagen density in aged 11 $\beta$ -HSD1-null mice. Collagen staining intensity appeared greater in aged KO (B) versus WT (A) mouse skin sections, contributing to the improved structural appearance in these mice. (C) Quantification of staining confirmed an increased collagen density in aged KO versus WT mice ( $n = 4$ ), with a similar trend in young mice ( $n = 4$ ). Scale bars: 50  $\mu$ M. \* $P < 0.05$ .



**Table 1**

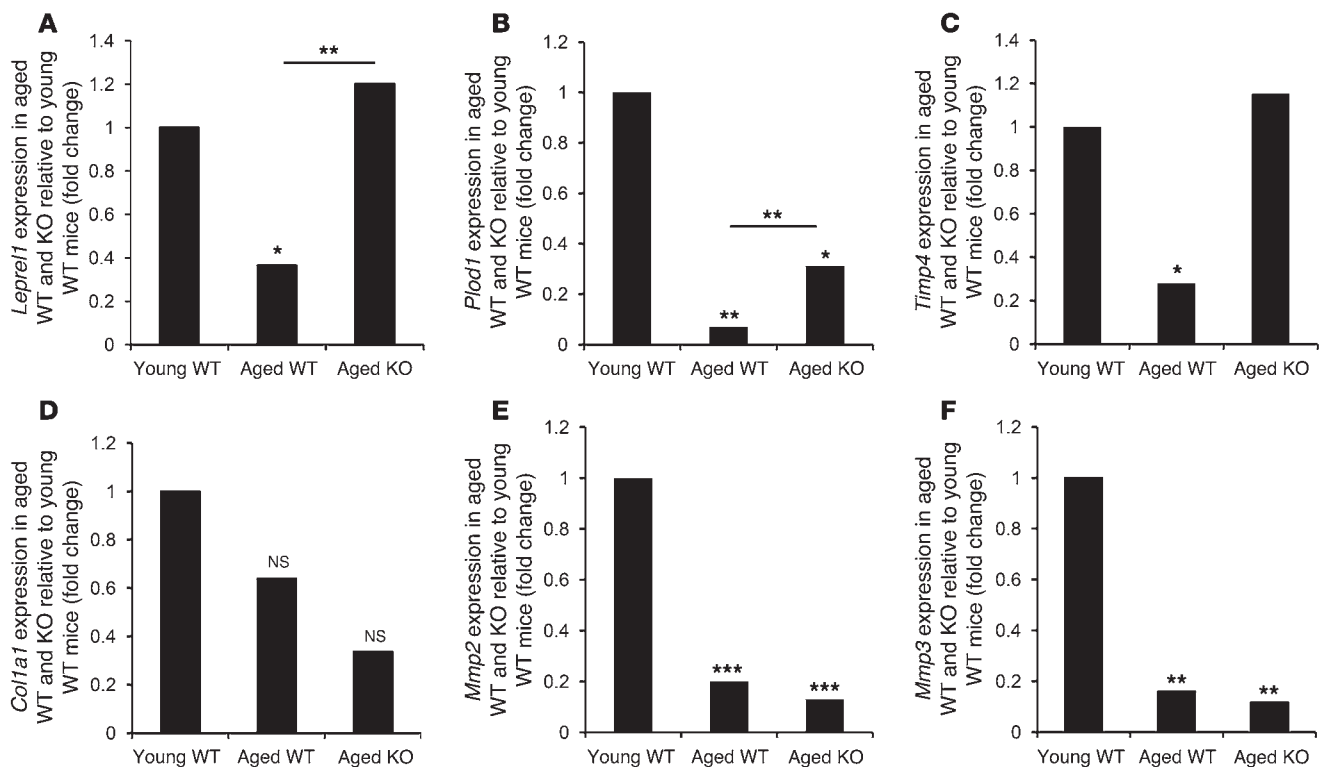
GC-regulated target genes in cultured fibroblasts impair collagen biosynthesis and processing

Gene symbol	Gene title	Function	Fold change	P value
<b>Pre-propeptide expression</b>				
<i>COL1A1</i>	Collagen type 1, alpha 1	Primary matrix structural component	0.64	0.078
<i>COL3A1</i>	Collagen type 3, alpha 1	Secondary matrix structural component	0.95	0.57
<i>PEPD</i>	Peptidase D	Proline recycling	0.87	0.18
<b>Procollagen assembly</b>				
<i>LEPRE1</i>	Leucine proline-enriched proteoglycan (leprecan) 1	Intrafibril stability	0.84	0.059
↓ <i>LEPREL1</i>	Leprecan-like 1	Intrafibril stability	0.2	<sup>B</sup>
↓ <i>LEPREL2</i>	Leprecan-like 2	Intrafibril stability	0.67	<sup>B</sup>
<i>P4HA1</i>	Prolyl 4-hydroxylase, alpha polypeptide 1	Intrafibril stability	0.8	0.14
↓ <i>P4HA2</i>	Prolyl 4-hydroxylase, alpha polypeptide 2	Intrafibril stability	0.64	<sup>A</sup>
<i>P4HA3</i>	Prolyl 4-hydroxylase, alpha polypeptide 3	Intrafibril stability	1.29	0.25
<i>P4HB</i>	Prolyl 4-hydroxylase, beta polypeptide	Intrafibril stability	0.78	0.07
<i>PLOD1</i>	Procollagen-lysine, 2-oxoglutarate 5-dioxygenase 1	Intrafibril stability	0.84	0.081
↓ <i>PLOD2</i>	Procollagen-lysine, 2-oxoglutarate 5-dioxygenase 2	Intrafibril stability	0.47	<sup>A</sup>
<i>PLOD3</i>	Procollagen-lysine, 2-oxoglutarate 5-dioxygenase 3	Intrafibril stability	0.92	0.45
<b>Procollagen transport</b>				
↓ <i>SERPINH1</i>	Serpin peptidase inhibitor, clade H (heat shock protein 47), member 1, (collagen binding protein 1)	Collagen chaperone	0.81	<sup>B</sup>
<b>Tropocollagen formation</b>				
<i>ADAMTS2</i>	ADAM metalloproteinase with thrombospondin type 1 motif, 2	N-propeptide cleavage	0.96	0.58
<i>BMP1</i>	Bone morphogenetic protein 1	C-propeptide cleavage	1.28	0.17
<b>Collagen fibril organization</b>				
↓ <i>LOX</i>	Lysyl oxidase	Interfibril cross-linking	0.69	<sup>A</sup>
↓ <i>LOXL1</i>	Lysyl oxidase-like 1	Interfibril cross-linking	0.47	<sup>B</sup>
↓ <i>LOXL2</i>	Lysyl oxidase-like 2	Interfibril cross-linking	0.58	<sup>A</sup>
↓ <i>LOXL3</i>	Lysyl oxidase-like 3	Interfibril cross-linking	0.54	<sup>C</sup>
↓ <i>LOXL4</i>	Lysyl oxidase-like 4	Interfibril cross-linking	0.59	<sup>A</sup>
↑ <i>DCN</i>	Decorin	Interfibril cross-linking	2.71	<sup>B</sup>
<b>Collagen fibril remodeling</b>				
↓ <i>MMP1</i>	Matrix metalloproteinase 1 (interstitial collagenase)	Cleaves collagen I, II, III VII and X	0.29	<sup>C</sup>
<i>MMP2</i>	Matrix metalloproteinase 2 (gelatinase A, 72 kDa gelatinase, 72 kDa type IV collagenase)	Cleaves collagen IV	0.87	0.2
<i>MMP3</i>	Matrix metalloproteinase 3 (stromelysin 1, progelatinase)	Cleaves fibronectin, laminin, gelatin I, III, IV, and V, collagen III, IV, X, and IX and cartilage proteoglycans. Activates procollagenase.	0.76	0.14
<i>MMP8</i>	Matrix metalloproteinase 8 (neutrophil collagenase)	Cleaves collagen I, II and III	2.3	0.066
<i>MMP10</i>	Matrix metalloproteinase 10 (stromelysin 2)	Cleaves fibronectin, gelatin of I, III, IV, and V and weakly collagens III, IV, and V	0.41	0.084
↓ <i>MMP12</i>	Matrix metalloproteinase 12 (macrophage elastase)	Cleaves elastin	0.56	<sup>A</sup>
<i>MMP13</i>	Matrix metalloproteinase 13 (collagenase 3)	Cleaves collagen II, I, and III	–	–
<i>TIMP1</i>	TIMP metalloproteinase inhibitor 1	Inhibits MMP1-3, 7-13 and 16	0.93	0.29
<i>TIMP2</i>	TIMP metalloproteinase inhibitor 2	Inhibits MMP1-3, 7-10, 13-16 and 19	0.84	0.22
↓ <i>TIMP3</i>	TIMP metalloproteinase inhibitor 3	Inhibits MMP1-3, 7 and 9	0.36	<sup>B</sup>
↑ <i>TIMP4</i>	TIMP metalloproteinase inhibitor 4	Inhibits MMP1-3, 7, 9 and 13-16	4.61	<sup>C</sup>

Treatment of primary HDFs with 100 nM cortisol downregulated mRNA expression of key mediators of collagen fibril assembly, transport, extracellular cross-linking and remodeling ( $n = 5$ ). <sup>A</sup> $P < 0.05$ ; <sup>B</sup> $P < 0.01$ ; <sup>C</sup> $P < 0.001$ .

ing GC treatment. Following secretion into the extracellular environment, the nonhelical procollagen “ends” are cleaved by membrane-bound collagen peptidases (ADAMTS2 and BMP1), which did not appear to be GC regulated. The resulting tropocollagen peptides are cross-linked by lysyl oxidases (LOX and LOXL1-4), which use lysine and hydroxylysine residues to form covalent bonds in the resultant collagen fibril. Interestingly,

mRNA expression for all 5 lysyl oxidases was reduced by GC treatment, with decreases ranging from 31% to 53%. The stability of collagen fibrils is further supported by proteoglycans such as decorin (DCN), which displayed a 2.7-fold induction of mRNA expression following GC treatment. Collagen-degrading MMPs and their inhibitors were also GC regulated, with reduced expression of MMP1 (71%), MMP12 (44%), and TIMP3 (64%)

**Figure 5**

Improved collagen synthesis gene expression in aged  $11\beta$ -HSD1-null mice. (A) Expression of the prolyl hydroxylase LEPREL1 decreased in the aged WT mice ( $n = 3$ ) relative to the younger animals ( $n = 5$ ). This was reversed in the aged KO mice ( $n = 4$ ). (B) Similarly, the age-induced decrease in lysyl hydroxylase PLOD1 expression was partially rescued in aged KO mice. (C) TIMP4 expression was also reduced in aged WT, but not KO, mice relative to young WT mice. (D) COL1A1 expression was unaltered with age or genotype. (E and F) An age-induced decrease in MMP2 and MMP3 was also observed but was unaffected by genotype. \* $P < 0.05$ ; \*\* $P < 0.01$ ; \*\*\* $P < 0.001$ . NS, nonsignificant.

and a 4.6-fold induction of TIMP4. We found that MMP8 and MMP10 also displayed a trend toward GC-mediated induction and reduction, respectively.

*Age-induced changes in collagen biosynthesis gene expression are rescued in  $11\beta$ -HSD1 KO mice.* In mouse skin, collagen (*Col1a1*) expression was unaffected by age or  $11\beta$ -HSD1 genotype (Figure 5D), but we found a 64% age-induced decrease in mouse skin prolyl hydroxylase (*Leprel1*) expression, which was fully restored in aged  $11\beta$ -HSD1 KO mice to levels comparable to those of young animals (Figure 5A). Similarly, a greater than 90% decrease in lysyl hydroxylase (*Plod1*) expression in aged WT skin was also partially rescued in the KO littermates (Figure 5B).

*Timp4* expression was also decreased by approximately 80% in the aged WT mice, but not in the KO mice (Figure 5C). By contrast, the age-induced downregulation of *Mmp2* and *Mmp3* expression was unaltered in the KO animals (Figure 5, E and F).

*Local blockade of endogenous GC activation accelerates wound healing in vivo.* Body weight at each time point was indistinguishable between the vehicle- and inhibitor-treated groups (data not shown). Gross wound morphology revealed accelerated closure in  $11\beta$ -HSD1 inhibitor-treated mice (Figure 6A). Indeed, accelerated re-epithelialization (ranging from 35% to greater than 100%) was observed in inhibitor-treated animals at each time point measured. For example, the area of neopidermis at 14 days after wounding was 23% in the vehicle-treated mice, but increased to 50% following  $11\beta$ -HSD1 blockade ( $P < 0.001$ ;  $n = 12$ ) (Figure 6B). Moreover,

while vehicle-treated mice required 18 days to reach 40% re-epithelialization,  $11\beta$ -HSD1 blockade reduced this time by over a week, attaining a similar level of recovery by day 9.

Importantly, we also observed faster wound closure in the aged  $11\beta$ -HSD1 KO mice compared with their WT littermates (Figure 7A).  $11\beta$ -HSD1 KO wound areas were reduced by approximately 50% at 4 days ( $P < 0.05$ ,  $n = 6$ ), while WT wound areas were still comparable to those on day 0, with a similar trend observed on day 2 (Figure 7B).

## Discussion

Our previous studies reported an increase in  $11\beta$ -HSD1 expression in HDFs obtained from older compared with younger donors and in PE cells relative to donor-matched PP cells in culture (26). Here, we provide new evidence that these in vitro observations translate into increased  $11\beta$ -HSD1 expression and activity in aging skin both in humans and mice. Our data support a role for  $11\beta$ -HSD1 in both intrinsic (e.g., PP skin) and “accelerated” extrinsic aging (e.g., PE skin); with increased  $11\beta$ -HSD1 expression and activity in PE skin further exacerbating the age-induced increase in PP skin.

The increased  $11\beta$ -HSD oxoreductase activity measured in our human cohort reflects the “net” effect of both  $11\beta$ -HSD isozymes resulting from increased  $11\beta$ -HSD1 or, alternatively, from decreased  $11\beta$ -HSD2. Our findings demonstrating increased  $11\beta$ -HSD1 protein in PE human skin and increased oxoreductase activity in aging mouse skin (devoid of  $11\beta$ -HSD2 activity and expression) confirm that altered levels of the type 1

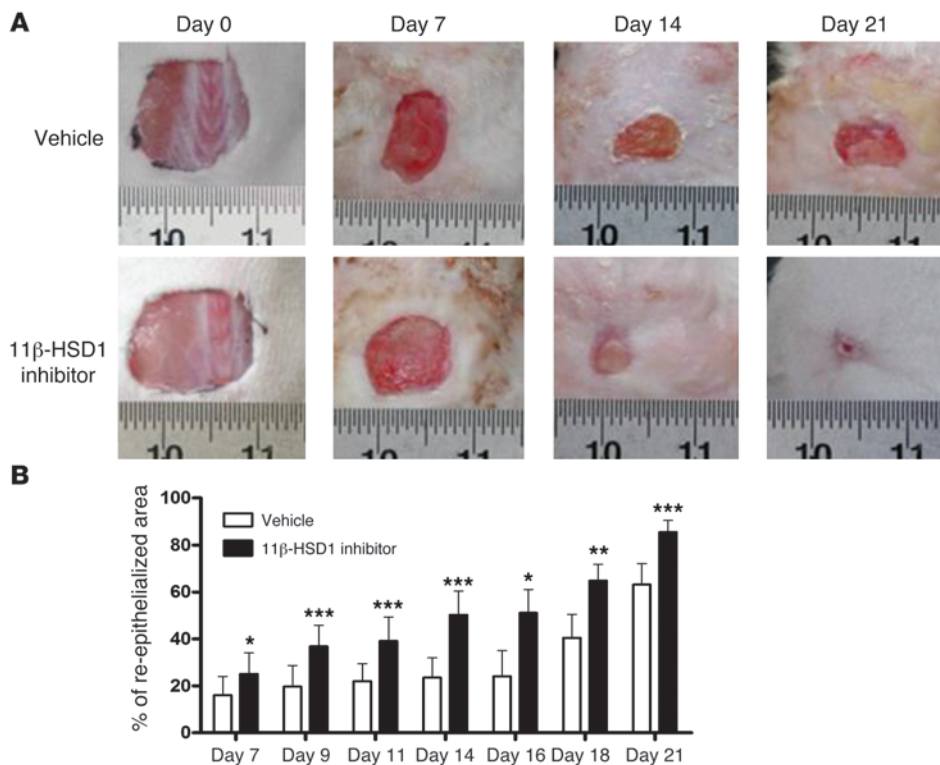


**Figure 6** Accelerated wound healing in 11β-HSD1 inhibitor–treated mice. (A) Representative images showing improved wound closure in mice treated every 2–3 days with 1% RO151. (B) Accelerated re-epithelialization was recorded at each time point measured (*n* = 5–12). \**P* < 0.05; \*\**P* < 0.01; \*\*\**P* < 0.001.

isozyme are exclusively responsible. Immunohistochemical studies in human skin demonstrated 11β-HSD1 staining predominantly in PP epidermis, with increased staining in photo-aged keratinocytes in addition to induced expression in PE dermal fibroblasts. Although our subsequent studies focused primarily on the dermal consequences of age-induced increased 11β-HSD1 activity, our observation suggests that both cell types contribute to this increase. Further studies should elucidate whether impaired epidermal function in aged skin is also a consequence of increased GC activation.

To the best of our knowledge, our group was the first to report an association between 11β-HSD1 and aging using primary human osteoblasts (27). Subsequently, a growing body of evidence has suggested that the age-related increase in 11β-HSD1 occurs in a variety of cells and tissues, including lymphocytes (28), bone (29), brain (30), and adipose (31), implicating a role for 11β-HSD1 in systemic aging. In these tissues, increased local GC activation is postulated to contribute to the increased risk of fracture and osteoporosis and impaired cognitive function associated with aging. Improved cognition and increased long-term potentiation have been reported in aged 11β-HSD1 KO mice relative to age-matched controls (32), with improved memory consolidation, recall, and social recognition also reported following treatment with specific 11β-HSD1 inhibitors (33, 34).

Our results also demonstrate that increased 11β-HSD1 activity is in part responsible for the phenotypic consequences of aging skin, with aged 11β-HSD1 KO mice displaying a reversal in age-induced dermal atrophy and structural disorganization

with increased collagen density. If translated to humans, these effects may lead to improvements in skin function in the elderly. Studies have shown a close relationship between the ECM microenvironment (including mechanical properties of young relative to aged collagen) and synthesis of molecules that regulate cell-ECM attachment, repair, and turnover by resident dermal fibroblasts (18, 24, 35, 36). Moreover, degraded ECM is central to facilitating tumor metastasis (37, 38), suggesting that preventing or limiting local GC activation may also reduce skin cancer risk. Our studies of HDFs treated with physiological concentrations of endogenous cortisol were designed to further investigate the potential mechanisms contributing to the improvements in collagen organization in aged 11β-HSD1 KO mice. We identified several previously unreported GC-regulated genes in HDFs underpinning the key stages of collagen biosynthesis and processing (Figure 8). These include the reduced expression of enzymes involved in procollagen hydroxylation (required for correct

molecular assembly), intracellular transport, and extracellular cross-linking, which may explain the collagen atrophy observed in our studies and reported by others (39).

Reduced expression of prolyl hydroxylases by GC in skin was previously limited to studies in rats (40, 41). Recently, Vranka et al. characterized the phenotype of the prolyl 3-hydroxylase 1-null (LEPRE1-null) mouse which, in addition to bone and tendon abnormalities, displayed a less densely packed dermis, with fewer collagen fibrils in the skin of newborn KO mice and skin thinning in adults, with collagen fibril clumping and interfibril spaces (42). These findings are endorsed by mutations in LEPRE1 in humans, which cause a recessive metabolic bone disorder resembling lethal/severe osteogenesis imperfecta (43), with patients also exhibiting overmodification of type I procollagen chains in dermal fibroblast cultures from affected individuals (44).

Mutations in genes encoding lysyl hydroxylases are known to cause Ehlers-Danlos syndrome type VI, characterized by neonatal kyphoscoliosis, generalized joint laxity, skin fragility, and severe muscle hypotonia at birth (45), as well as Bruck syndrome (46), affecting bone collagen cross-linking (47), with overexpression associated with skin fibrosis (46). Our results show a decrease in the expression of all 5 known lysyl oxidase isozymes following GC treatment, in agreement with previous rodent studies evaluating the effect of local GC treatment (41). Decreased lysyl oxidase activity has been identified as a cause of Ehlers-Danlos syndrome variant type IX and the clinically distinct Menkes syndrome, both manifesting with skin laxity and hyperextensibility (48).

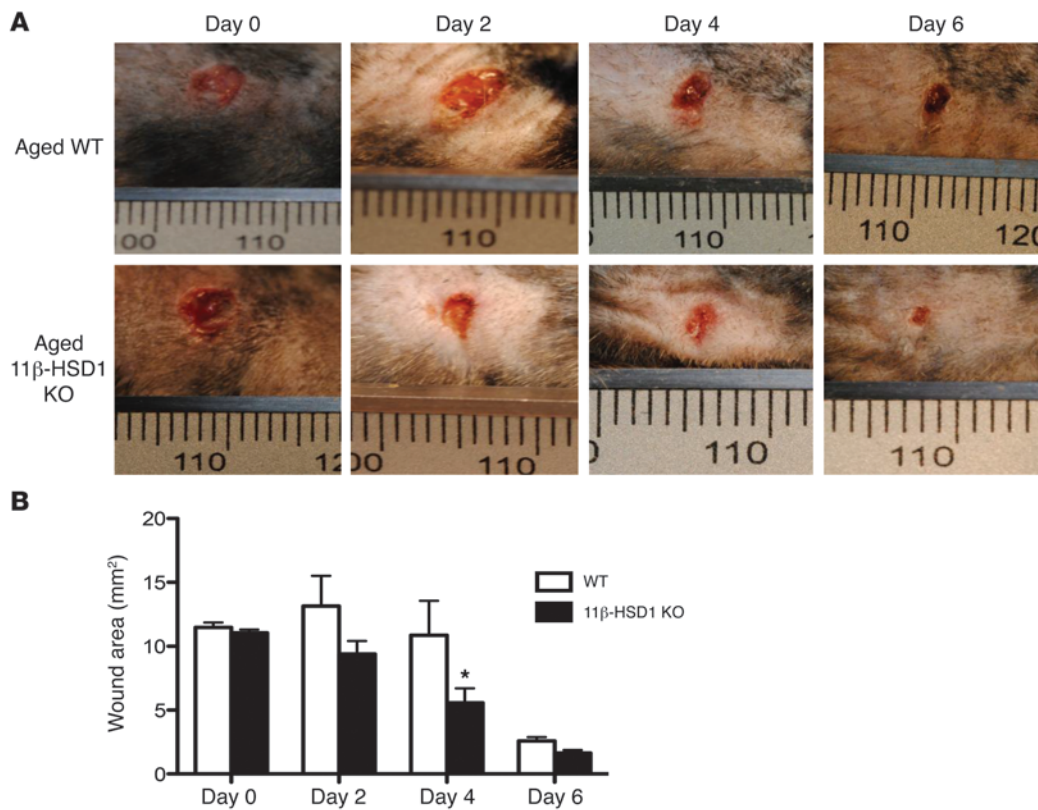


**Figure 7**

Accelerated healing in aged 11 $\beta$ -HSD1 KO mice. (A) Representative images showing accelerated wound closure in aged 11 $\beta$ -HSD1 KO mice. (B) Increased healing was observed at 4 days, with a similar trend at 2 days ( $n = 6$ ). \* $P < 0.05$ .

We also report GC-induced differential regulation of several enzymes involved in collagen turnover and remodeling, including downregulation of MMP1, the elastin-degrading MMP12 as previously reported (49, 50), and a similar trend for MMP10. Conversely, TIMP4, a potent inhibitor of the type IV collagenase MMP2 (51), was upregulated, whereas an opposing effect was observed for TIMP3. Although still poorly understood, altered expression of these highly complex mediators of collagen remodeling through increases in local GC availability are likely to play an important role in aging skin phenotype manifestation. Collectively, the identification of these critical regulators of collagen biosynthesis as novel GC targets in HDF raises the possibility that altered local GC availability could contribute to several aspects of altered collagen structural organization in aging skin.

Subsequently, we analyzed the expression of GC-regulated genes in our KO mouse model and showed a reversal of age-related decreases in *Leprel1*, *Plod1* and *Timp4* expression. Procollagen type 1 expression (*Col1a1*) was largely unaffected by age or genotype, suggesting that altered posttranslational processing and remodeling, rather than decreased collagen synthesis, may be responsible for the age-induced changes in dermal structure, as previously proposed by others (52). Furthermore, the decreased expression of *Mmp2* and *Mmp3* in older WT mice was maintained in the KO animals, suggesting that a specific subset of collagen biosynthesis and remodeling genes may be involved in the etiology of skin aging.

These findings suggest that blockade of the age-related increase in 11 $\beta$ -HSD1 activity may promote improved structural and functional properties in aging skin. Selective 11 $\beta$ -HSD1 inhibitors have already been deployed by many pharmaceutical companies, largely on the premise that they may reverse or prevent obesity-related diabetes mellitus (53–57). Our collaborative research using a highly selective and effective 11 $\beta$ -HSD1 inhibitor, RO151, demonstrates accelerated re-epithelialization and wound healing and presents the exciting possibility that topical 11 $\beta$ -HSD1 inhibitors might be used to combat age-related impairments in wound healing. Our observation that aged 11 $\beta$ -HSD1 KO mice exhibit accelerated wound healing relative to WT littermates further supports this possibility.

Although the central theme of the current research focused on chronological aging, our finding demonstrating elevated 11 $\beta$ -HSD1 activity and expression in PE skin presents 11 $\beta$ -HSD1 as a candidate indicator of photo-aging and extends the scope of pharmacological intervention and/or treatment to photo-damaged skin. Finally, our studies may have implications in the context of slow-healing wounds occurring in diabetics or sufferers of chronic stress, where limiting local GC generation could also improve healing.

## Methods

Materials were purchased from Sigma-Aldrich unless otherwise stated.

### Tissue preparation and cell culture

**Human tissue.** A group of 40 healthy Caucasians consisting of 20 young (year  $\pm$  SD, 25.7  $\pm$  3.0; 9 female and 11 male) and 20 older (72.2  $\pm$  8.2; 11 female and 9 male) donors underwent 3-mm biopsies of PE (lower outer) and PP (inner upper) arm skin. The skin was sterilized and covered with Supadrape (Westfield Medical Ltd.) containing a central aperture prior to local anesthetic injection with 2 ml of 2% lidocaine HCl (National Veterinary Services). Following dispersion, skin was tested for numbness before obtaining 2 biopsies per site using a Stiefel 3-mm Biopsy Punch (Medisave). Cotton gauze was used to contain bleeding before Inadine patch and Mepore dressing application (Oncall Medical Supplies). Tissue was stored in complete media (RPMI-1640, 10% FCS, 2 mM L-glutamine, 1% Pen-Strep, 1% sodium pyruvate, and 1% nonessential amino acids) and either analyzed immediately or snap-frozen and stored at  $-80^{\circ}\text{C}$ .

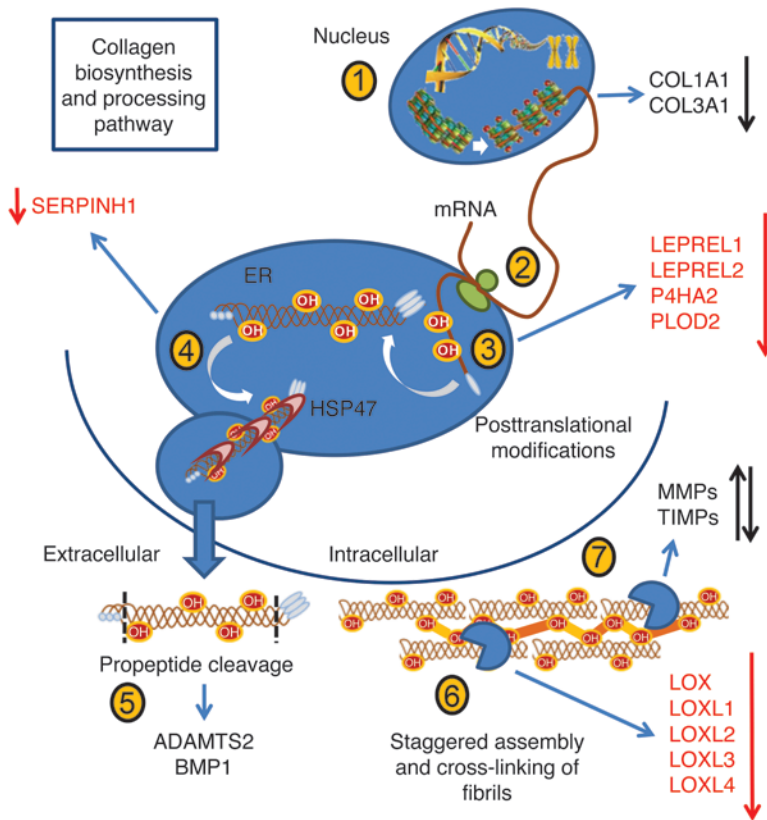


**Figure 8**  
GC treatment impairs multiple elements of collagen biosynthesis and processing. GC treatment of primary HDFs decreased collagen transcription (1) and altered collagen metabolizing enzymes (7) as previously shown. We found additional GC targets, including reduced expression of collagen posttranslational hydroxylation enzymes (3), collagen chaperone (4), and all lysyl oxidase enzyme isoforms required for collagen inter- and intrafibril cross-link formation (6).

**Mouse tissue.** Studies were conducted as previously described (26). Mouse skin from male young (11–20 weeks of age,  $n = 10$ ) and aged (91–99 weeks of age,  $n = 5$ ) WT mice and from littermates with global deletion of 11 $\beta$ -HSD1 (generated in-house;  $n = 15$ ) (58) was obtained by dissection of shaved skin from the lower dorsal region. 11 $\beta$ -HSD1 KO mice were backcrossed (greater than 9 generations) into C57BL6/J mice, with appropriate strain controls used.

**HDF culture and treatment.** HDFs were cultured from lower outer arm biopsies from Caucasian donors of variable age by incubation for 8 days at 37°C in a 5% CO<sub>2</sub> atmosphere in T25 flasks containing 2 ml of complete media.

Upon attaining 80% confluence, cells were passaged at a ratio of 1:3 as required. For GC treatment, cells were seeded into 6-well plates at 70% confluence and incubated overnight. Cells were treated with 100 nM cortisol (in duplicate) for 48 hours and compared with vehicle-treated controls.

**11 $\beta$ -HSD1 activity assays**

One biopsy per site per human donor (~4–10 mg) was analyzed for 11 $\beta$ -HSD1 (oxoreductase) activity. Mouse skin explants (~6 mg) were analyzed in duplicate. Intact tissue activity was measured in 10-ml glass tubes containing 0.5 ml of complete media, 100 pmol of cortisone or 11-dehydrocorticosterone for human and mouse skin, respectively, and tracer amounts of [<sup>3</sup>H] cortisone or 11-dehydrocorticosterone as previously reported (26). For human tissue, activity was expressed as the percentage of conversion

of cortisone to cortisol (24 hours). In these samples, activity was not normalized for tissue weight – which was increased in PE samples (Supplemental Figure 1A; supplemental material available online with this article; doi:10.1172/JCI64162DS1), owing to a deeper dermal layer composed primarily of inert structural proteins, e.g., collagen – as this did not correlate with enzyme activity in either group (Supplemental Figure 1B). Furthermore, punch biopsies standardized the same surface area between samples. For mouse samples, enzyme activity was normalized for tissue weight (pmol corticosterone/mg tissue/h) as surface area varied.

**Immunohistochemistry**

11 $\beta$ -HSD1 protein detection in frozen human skin sections (fixed in 3:1 acetone/ethanol) was analyzed by immunohistochemistry using a primary mAb (Abcam) and an alkaline phosphatase-conjugated goat anti-mouse secondary Ab (Dako). Fast Red TR/Naphthol AS-MX Tablets were used to visualize the staining according to the manufacturer’s guidelines. Briefly, slides were incubated for 15 minutes in 56:1 methanol/hydrogen peroxide to inactivate endogenous peroxidases, rinsed with deionized water, and blocked for 1 hour in TBSAT (10 ml 10 $\times$  TBS [121.2 g Tris/160.4 g sodium chloride, pH 7.6, in 2 liters of deionized water], stored in aliquots at –20°C), 3 g of BSA, 50  $\mu$ l of Triton X100, and 10% goat serum. Slides were drained and incubated for 2 hours in fresh TBSAT with the primary Ab diluted 1:100 before washing under agitation in three 10-minute washes of TBST (~800 ml 1 $\times$  TBS plus 0.05% Tween-20). Slides were drained and incubated for 30 minutes in fresh TBSAT with the secondary Ab diluted 1:200 before repeating washes. Following visualization, slides were air-dried before applying aqueous mounting medium and coverslips. Staining was observed in similar structures to those previously described using a polyclonal Ab (26) and was negligible when substituting equimolar concentrations of isotype control (mouse IgM; AbCam) for the primary Ab (Supplemental Figure 2).

Sections were photographed using a Nuance multispectral imaging system (CRi, Advanced Molecular Vision). Nuance image analysis software was used to annotate the DEJ and stratum corneum-granulosum interface (CRi, Advanced Molecular Vision). Staining intensity was measured in the epidermis and upper dermis.

**Histology**

Tissue was stored in 10% neutral buffered formalin (4 g sodium monophosphate, 6.5 g sodium diphosphate in 900 ml of distilled water, and 100 ml of 37% formaldehyde) before paraffin embedding and sectioning. Paired sections from each age and genotype were cut per slide. Following dewaxing and rehydration (26), the slides were stained with H&E, mounted, coverslipped, and analyzed in a blinded fashion by 2 independent researchers. Sections were stained for collagen using a Masson trichrome kit according to the manufacturer’s guidelines. Collagen stain intensity was determined using the Nuance system described above.

**RNA extraction and reverse transcription**

Total RNA was extracted from primary cultures of HDFs using the Tri-Reagent method (Sigma-Aldrich), with generation of cDNA by reverse transcription as previously described (26). Tissue RNA was extracted using an RNeasy Fibrous Tissue kit (QIAGEN) using a PowerGen 125 homogenizer (Fisher Scientific) according to the manufacturer’s protocol.



### Real-time PCR gene expression analysis

**HDF studies.** The BioMark system (Fluidigm) was used to analyze the expression of 33 genes involved in collagen biosynthesis and processing. Specific target preamplification was conducted in 5- $\mu$ l volumes consisting of a 2.5- $\mu$ l TaqMan PreAmp Master Mix (2 $\times$ ; Applied Biosystems), a 1.25- $\mu$ l pooled TaqMan gene expression assay (1  $\mu$ l for each assay and 4  $\mu$ l 1 $\times$  TE buffer, 0.2 $\times$  final assay concentration), and 1.25  $\mu$ l (25–50 ng) of cDNA (or 1 $\times$  TE for the negative control). Following brief vortexing and centrifugation, samples were heated to 95°C for 10 minutes followed by 14 cycles of 95°C for 15 seconds and 60°C for 4 minutes. Samples were then diluted 1:5 with 20  $\mu$ l of 1 $\times$  TE buffer. Following preamplification, 1  $\mu$ l of each sample was also pooled and serially diluted in 1 $\times$  TE buffer (1:10, 1:100, 1:1,000, and 1:10,000) for standard curve generation.

Samples (in triplicate) and standards (in duplicate) were prepared for loading onto the chip in 8- $\mu$ l volumes in a 96-well plate: 4  $\mu$ l of TaqMan Universal PCR Master Mix (2 $\times$ ); 0.4  $\mu$ l of GE Sample Loading Reagent (20 $\times$ , Fluidigm); and 3.6  $\mu$ l of preamplified cDNA per standard. Plates were vortexed, centrifuged, and stored at 5°C until required. Gene expression assays were prepared in 8- $\mu$ l volumes: 4  $\mu$ l of TaqMan Gene Expression Assay (20 $\times$ ) and 4  $\mu$ l of Assay Loading Reagent (2 $\times$ ; Fluidigm), giving final concentrations of 9  $\mu$ M and 2.5  $\mu$ M for the primers and probe per assay, respectively. Samples were vortexed, centrifuged and stored at 5°C. Chips were primed using the IFC controller according to the manufacturer's protocol (Fluidigm), loaded with 5  $\mu$ l of Sample Mix, 5  $\mu$ l of Assay Mix, and activated using the IFC controller. Chips were processed on a BioMark quantitative PCR reader (Fluidigm). Following standard curve verification,  $\Delta$ Ct values were determined for each sample by normalizing to the geometric mean of 4 housekeeper genes (*RPL13*, *TBP*, *B2M*, and *PPIA*). Mouse tissue: *Leprel1*, *Plod1*, *Timp4*, *Col1a1*, *Mmp2*, and *Mmp3* mRNA levels were measured (in duplicate) by conventional real-time PCR using an ABI 7500 system (PerkinElmer). PCR was performed in 10- $\mu$ l reactions in 96-well plates. Reactions contained 5  $\mu$ l of 2 $\times$  TaqMan Universal PCR Mastermix, 0.5  $\mu$ l of assay (900 nM primer and 250 nM probe final concentrations), 3.5  $\mu$ l of distilled water, and 1  $\mu$ l of cDNA (25–50 ng). Reactions were standardized to the housekeeper 18S (all Applied Biosystems). Reactions were as follows: 50°C for 2 minutes, 95°C for 10 minutes, 40 cycles of 95°C for 15 seconds, and 60°C for 1 minute.

### Wound-healing studies

**11 $\beta$ -HSD1 inhibitor studies.** Inhibitor studies were conducted in 8-week-old male Swiss mice ( $n = 5–12$ ) using RO151, known to selectively inhibit 11 $\beta$ -HSD1 activity in vivo (59), with an IC<sub>50</sub> of 40 nM ( $\pm 4$  nM SE;  $n = 17$ ) against the murine homolog (determined by cellular assays using 3T3-L1 adipocytes; data not shown). One percent RO151 was formulated in 9.1% hydroxypropyl beta cyclodextrin, 0.5% Tris, and 0.45% sodium chloride (pH 7.3) before 3% hydroxypropyl methyl cellulose was added at room temperature under agitation to produce a clear gel.

Full-thickness dorsal wounds of approximately 10 mm<sup>2</sup> were created under ketamine-xylazine anesthesia. The gel containing 11 $\beta$ -HSD1 inhibitor and vehicle was applied and covered with OpSite Flexifix (Smith &

Nephew) and Hypafix tape (BSN Medical). Applications were repeated every 2–3 days until 21 days after wounding. Wound photographs and body weight measurements were taken at each time point. Wound healing is presented as the re-epithelialized area measured by subtracting the area uncovered by neoepidermis from the original wound area calculated using ImageJ software (NIH).

**11 $\beta$ -HSD1 KO studies.** Aged male 11 $\beta$ -HSD1 KO (52 weeks of age  $\pm$  0.68 SD) and WT (51 weeks of age  $\pm$  0.67 SD) mice ( $n = 6$ ) were anesthetized and shaved before a 4-mm full-thickness skin punch biopsy was performed on the right side of the thorax using a biopsy punch (Acuderm). Wounds were photographed at 0, 2, 4, and 6 days after the biopsy was measured as above.

### Statistics

Experimental data were analyzed using GraphPad Prism software (GraphPad). A Student's *t* test was used to compare data displaying a normal distribution (paired tests were used as appropriate). Wound-healing studies in aged 11 $\beta$ -HSD1 KO mice were assessed using 2-way ANOVA (SigmaStat 3.1). Data represent the means  $\pm$  SEM. The null hypothesis was rejected at a significance level of  $P < 0.05$ , with data values as follows: \* $P < 0.05$ ; \*\* $P < 0.01$ ; and \*\*\* $P < 0.001$ .

### Study approval

Animal studies were conducted under Home Office license and following approval of the Joint Ethics and Research Governance Committee of the University of Birmingham (Birmingham, United Kingdom) in accordance with the UK Animals (Scientific Procedures) Act, 1986. Human studies were conducted following ethical approval (Black Country Research Ethics Committee, Manchester, United Kingdom) and according to the Declaration of Helsinki Principles. All participants gave their written informed consent before study enrolment.

### Acknowledgments

This work was supported through a BBSRC Case PhD studentship. Additional support was provided from a Wellcome Trust Programme Grant, an ERC Advanced Research Fellowship (to P.M. Stewart), and a BBSRC David Philips fellowship to Gareth Lavery (BB/G023468/1). M. Otranto holds a doctoral fellowship from Fundação de Amparo à Pesquisa do Estado do Rio de Janeiro, Brazil. We are grateful to Nelly Bordeau (Department of Physiology, University of Limoges, France) for technical help with wound-healing studies.

Received for publication November 19, 2012, and accepted in revised form March 28, 2013.

Address correspondence to: Paul M. Stewart, College of Medical and Dental Sciences, University of Birmingham, Birmingham B15 2TT, United Kingdom. Phone: 44.0.121.415.8708; Fax: 44.0.121.415.8712 or 44.0.121.414.7149; E-mail: p.m.stewart@bham.ac.uk.

1. Newell-Price J, Bertagna X, Grossman AB, Nieman LK. Cushing's syndrome. *Lancet*. 2006; 367(9522):1605–1617.
2. Korting HC, Unholzer A, Schafer-Korting M, Tausch I, Gassmueller J, Nietsch KH. Different skin thinning potential of equipotent medium-strength glucocorticoids. *Skin Pharmacol Appl Skin Physiol*. 2002;15(2):85–91.
3. Werth VP, Kligman AM, Shi XM, Pagnoni A. Lack of correlation of skin thickness with bone density in patients receiving chronic glucocorticoid. *Arch Dermatol Res*. 1998;290(7):388–393.
4. Sowers JR, Lippman HR. Cushing's syndrome due

- to ectopic ACTH production: cutaneous manifestations. *Cutis*. 1985;36(4):351–352.
5. Stenzel-Poore MP, Cameron VA, Vaughan J, Sawchenko PE, Vale W. Development of Cushing's syndrome in corticotropin-releasing factor transgenic mice. *Endocrinology*. 1992;130(6):3378–3386.
6. Faergemann J, et al. Dose-response effects of tri-iodothyroacetic acid (Triac) and other thyroid hormone analogues on glucocorticoid-induced skin atrophy in the haired mouse. *Acta Derm Venereol*. 2002;82(3):179–183.
7. Kimura T, Doi K. Dorsal skin reactions of hairless dogs to topical treatment with corticosteroids. *Toxicol Pathol*. 1999;27(5):528–535.
8. Nuutinen P, et al. Modulation of collagen synthesis and mRNA by continuous and intermittent use of topical hydrocortisone in human skin. *Br J Dermatol*. 2003;148(1):39–45.
9. Autio P, Oikarinen A, Melkko J, Risteli J, Risteli L. Systemic glucocorticoids decrease the synthesis of type I and type III collagen in human skin in vivo, whereas isotretinoin treatment has little effect. *Br J Dermatol*. 1994;131(5):660–663.
10. Oishi Y, Fu ZW, Ohnuki Y, Kato H, Noguchi T. Molecular basis of the alteration in skin collagen metabolism in response to in vivo dexamethasone



- treatment: effects on the synthesis of collagen type I and III, collagenase, and tissue inhibitors of metalloproteinases. *Br J Dermatol*. 2002;147(5):859–868.
11. Schoepe S, Schacke H, May E, Asadullah K. Glucocorticoid therapy-induced skin atrophy. *Exp Dermatol*. 2006;15(6):406–420.
  12. Lee B, Vouthounis C, Stojadinovic O, Brem H, Im M, Tomic-Canic M. From an enhanceosome to a repressosome: molecular antagonism between glucocorticoids and EGF leads to inhibition of wound healing. *J Mol Biol*. 2005;345(5):1083–1097.
  13. Mercado AM, Padgett DA, Sheridan JF, Marucha PT. Altered kinetics of IL-1 alpha, IL-1 beta, and KGF-1 gene expression in early wounds of restrained mice. *Brain Behav Immun*. 2002;16(2):150–162.
  14. Aberg KM, et al. Psychological stress downregulates epidermal antimicrobial peptide expression and increases severity of cutaneous infections in mice. *J Clin Invest*. 2007;117(11):3339–3349.
  15. Lavker RM. Structural alterations in exposed and unexposed aged skin. *J Invest Dermatol*. 1979;73(1):59–66.
  16. Varani J, et al. Vitamin A antagonizes decreased cell growth and elevated collagen-degrading matrix metalloproteinases and stimulates collagen accumulation in naturally aged human skin. *J Invest Dermatol*. 2000;114(3):480–486.
  17. Braverman IM, Fonferko E. Studies in cutaneous aging: I. The elastic fiber network. *J Invest Dermatol*. 1982;78:434–443.
  18. Varani J, et al. Decreased collagen production in chronologically aged skin – roles of age-dependent alteration in fibroblast function and defective mechanical stimulation. *Am J Pathol*. 2006;168(6):1861–1868.
  19. Liang JA, Pei XR, Zhang ZF, Wang N, Wang JB, Li Y. The protective effects of long-term oral administration of marine collagen hydrolysate from chum salmon on collagen matrix homeostasis in the chronological aged skin of Sprague-Dawley male rats. *J Food Sci*. 2010;75(8):H230–H238.
  20. Sayama A, Soushin T, Okada T, Doi K, Nakayama H. Morphological and biochemical changes during aging and photoaging of the skin of C57BL/6J mice. *J Toxicol Pathol*. 2010;23(3):133–139.
  21. Ghadially R, Brown BE, Sequeira Martin SM, Feingold KR, Elias PM. The aged epidermal permeability barrier. Structural, functional, and lipid biochemical abnormalities in humans and a senescent murine model. *J Clin Invest*. 1995;95(5):2281–2290.
  22. Escoffier C, Derigal J, Rochefort A, Vasselet R, Leveque JL, Agache PG. Age-related mechanical-properties of human-skin – an in vivo study. *J Invest Dermatol*. 1989;93(3):353–357.
  23. Ashcroft GS, Horan MA, Ferguson MWJ. Aging is associated with reduced deposition of specific extracellular matrix components, upregulation of angiogenesis, and an altered inflammatory response in a murine incisional wound healing model. *J Invest Dermatol*. 1997;108(4):430–437.
  24. Ballas CB, Davidson JM. Delayed wound healing in aged rats is associated with increased collagen gel remodeling and contraction by skin fibroblasts, not with differences in apoptotic or myofibroblast cell populations. *Wound Repair Regen*. 2001;9(3):223–237.
  25. Bearegard S, Gilchrist BA. A survey of skin problems and skin care regimens in the elderly. *Arch Dermatol*. 1987;123(12):1638–1643.
  26. Tiganescu A, Walker EA, Hardy RS, Mayes AE, Stewart PM. Localization, age- and site-dependent expression, and regulation of 11 $\beta$ -hydroxysteroid dehydrogenase type 1 in skin. *J Invest Dermatol*. 2011;131(1):30–36.
  27. Cooper MS, Rabbitt EH, Goddard PE, Bartlett WA, Hewison M, Stewart PM. Osteoblastic 11 beta-hydroxysteroid dehydrogenase type 1 activity increases with age and glucocorticoid exposure. *J Bone Miner Res*. 2002;17(6):979–986.
  28. Zhang TY, Ding XH, Daynes RA. The expression of 11 beta-hydroxysteroid dehydrogenase type I by lymphocytes provides a novel means for intracrine regulation of glucocorticoid activities. *J Immunol*. 2005;174(2):879–889.
  29. Weinstein RS, et al. Endogenous glucocorticoids decrease skeletal angiogenesis, vascularity, hydration, and strength in aged mice. *Aging Cell*. 2010;9(2):147–161.
  30. Holmes MC, et al. 11beta-hydroxysteroid dehydrogenase type 1 expression is increased in the aged mouse hippocampus and parietal cortex and causes memory impairments. *J Neurosci*. 2010;30(20):6916–6920.
  31. Andersson T, et al. Tissue-specific increases in 11beta-hydroxysteroid dehydrogenase type 1 in normal weight postmenopausal women. *PLoS One*. 2009;4(12):e8475.
  32. Yau JLW, et al. Enhanced hippocampal long-term potentiation and spatial learning in aged 11 beta-hydroxysteroid dehydrogenase type 1 knockout mice. *J Neurosci*. 2007;27(39):10487–10496.
  33. Sooy K, et al. Partial deficiency or short-term inhibition of 11beta-hydroxysteroid dehydrogenase type 1 improves cognitive function in aging mice. *J Neurosci*. 2010;30(41):13867–13872.
  34. Mohler EG, et al. Acute inhibition of 11beta-hydroxysteroid dehydrogenase type-1 improves memory in rodent models of cognition. *J Neurosci*. 2011;31(14):5406–5413.
  35. Damodarasamy M, et al. Collagen extracts derived from young and aged mice demonstrate different structural properties and cellular effects in three-dimensional gels. *J Gerontol A Biol Sci Med Sci*. 2010;65(3):209–218.
  36. Vedrenne N, Coulomb B, Danigo A, Bonté F, Desmoulière A. The complex dialogue between (myo)fibroblasts and the extracellular matrix during skin repair processes and aging. *Pathol Biol (Paris)*. 2012;60(1):20–27.
  37. Cretu A, Brooks PC. Impact of the non-cellular tumor microenvironment on metastasis: Potential therapeutic and imaging opportunities. *J Cell Physiol*. 2007;213(2):391–402.
  38. Willhauck MJ, et al. Reversion of tumor phenotype in surface transplants of skin SCC cells by scaffold-induced stroma modulation. *Carcinogenesis*. 2007;28(3):595–610.
  39. Bernstein EF, et al. Long-term sun exposure alters the collagen of the papillary dermis. Comparison of sun-protected and photoaged skin by northern analysis, immunohistochemical staining, and confocal laser scanning microscopy. *J Am Acad Dermatol*. 1996;34(2 pt 1):209–218.
  40. Cutroneo KR, Counts DF. Anti-inflammatory steroids and collagen metabolism: glucocorticoid-mediated alterations of prolyl hydroxylase activity and collagen synthesis. *Mol Pharmacol*. 1975;11(5):632–639.
  41. Benson SC, Luvall PA. Inhibition of lysyl oxidase and prolyl hydroxylase activity in glucocorticoid treated rats. *Biochem Biophys Res Commun*. 1981;99(2):557–562.
  42. Vranka JA, et al. Prolyl 3-hydroxylase 1 null mice display abnormalities in fibrillar collagen-rich tissues such as tendons, skin, and bones. *J Biol Chem*. 2010;285(22):17253–17262.
  43. Cabral WA, et al. Prolyl 3-hydroxylase 1 deficiency causes a recessive metabolic bone disorder resembling lethal/severe osteogenesis imperfecta. *Nat Genet*. 2007;39(3):359–365.
  44. Willaert A, et al. Recessive osteogenesis imperfecta caused by LEPRE1 mutations: clinical documentation and identification of the splice form responsible for prolyl 3-hydroxylation. *J Med Genet*. 2009;46(4):233–241.
  45. Yeowell HN, Walker LC. Mutations in the lysyl hydroxylase 1 gene that result in enzyme deficiency and the clinical phenotype of Ehlers-Danlos syndrome type VI. *Mol Genet Metab*. 2000;71(1–2):212–224.
  46. van der Slot AJ, et al. Identification of PLOD2 as telopeptide lysyl hydroxylase, an important enzyme in fibrosis. *J Biol Chem*. 2003;278(42):40967–40972.
  47. Bank RA, et al. Defective collagen crosslinking in bone, but not in ligament or cartilage, in Bruck syndrome: Indications for a bone-specific telopeptide lysyl hydroxylase on chromosome 17. *Proc Natl Acad Sci U S A*. 1999;96(3):1054–1058.
  48. Kuivaniemi H, Peltonen L, Kivirikko KI. Type IX Ehlers-Danlos syndrome and Menkes syndrome: the decrease in lysyl oxidase activity is associated with a corresponding deficiency in the enzyme protein. *Am J Hum Genet*. 1985;37(4):798–808.
  49. Bauer EA, Kronberger A, Valle KJ, Jeffrey JJ, Eisen AZ. Glucocorticoid modulation of collagenase expression in human skin fibroblast cultures. Evidence for pre-translational inhibition. *Biochim Biophys Acta*. 1985;825(2):227–235.
  50. Madlener M, Mauch C, Conca W, Brauchle M, Parks WC, Werner S. Regulation of the expression of stromelysin-2 by growth factors in keratinocytes: implications for normal and impaired wound healing. *Biochem J*. 1996;320:659–664.
  51. Bigg HF, et al. Tissue inhibitor of metalloproteinases-4 inhibits but does not support the activation of gelatinase A via efficient inhibition of membrane type I-matrix metalloproteinase. *Cancer Res*. 2001;61(9):3610–3618.
  52. Varani J, et al. Inhibition of type I procollagen synthesis by damaged collagen in photoaged skin and by collagenase-degraded collagen in vitro. *Am J Pathol*. 2001;158(3):931–942.
  53. Hollis G, Huber R. 11 beta-Hydroxysteroid dehydrogenase type 1 inhibition in type 2 diabetes mellitus. *Diabetes Obes Metab*. 2011;13(1):1–6.
  54. Feig PU, et al. Effects of an 11 beta-hydroxysteroid dehydrogenase type 1 inhibitor, MK-0916, in patients with type 2 diabetes mellitus and metabolic syndrome. *Diabetes Obes Metab*. 2011;13(6):498–504.
  55. Gibbs JP, et al. Population pharmacokinetic/pharmacodynamic model of subcutaneous adipose 11 $\beta$ -hydroxysteroid dehydrogenase type 1 (11 $\beta$ -HSD1) activity after oral administration of AMG 221, a selective 11 $\beta$ -HSD1 inhibitor. *J Clin Pharmacol*. 2011;51(6):830–841.
  56. Park JS, et al. Anti-diabetic and anti-adipogenic effects of a novel selective 11 beta-hydroxysteroid dehydrogenase type 1 inhibitor, 2-(3-benzoyl)-4-hydroxy-1,1-dioxo-2H-1,2-benzothiazine-2-yl-1-phenylethanolone (KR-66344). *Biochem Pharmacol*. 2011;81(8):1028–1035.
  57. Liu J, et al. Adipose tissue-targeted 11 beta-hydroxysteroid dehydrogenase type 1 inhibitor protects against diet-induced obesity. *Endocr J*. 2011;58(3):199–209.
  58. Semjonous NM, et al. Hexose-6-phosphate dehydrogenase contributes to skeletal muscle homeostasis independent of 11 $\beta$ -hydroxysteroid dehydrogenase type 1. *Endocrinology*. 2011;152(1):93–102.
  59. Fuerst-Recktenwald S, Abt M, Arlt W. Effects of two 11 $\beta$ -HSD1 inhibitors on the hypothalamic-pituitary-adrenal axis of male and female Type 2 diabetic patients. *Endocr Rev*. 2011;32(03\_Meeting-Abstracts):OR39-4.